Ground Validation for the Tropical Rainfall Measuring Mission (TRMM)

DAVID B. WOLFF,[*,+] D. A. MARKS,[*,#] E. AMITAI,[*,#] D. S. SILBERSTEIN,[*,#] B. L. FISHER,[*,+] A. TOKAY,[*,@] J. WANG,[*,+] AND J. L. PIPPITT[*,#]

[*]*Laboratory for Atmospheres, NASA Goddard Space Flight Center, Greenbelt, Maryland*
[+]*Science Systems & Applications, Inc., Lanham, Maryland*
[#]*Center for Earth Observing and Space Research, George Mason University, Fairfax, Virginia*
[@]*Joint Center for Earth Systems Technology, University of Maryland, Baltimore County, Baltimore, Maryland*

(Manuscript received 14 April 2004, in final form 4 August 2004)

ABSTRACT

An overview of the Tropical Rainfall Measuring Mission (TRMM) Ground Validation (GV) Program is presented. This ground validation (GV) program is based at NASA Goddard Space Flight Center in Greenbelt, Maryland, and is responsible for processing several TRMM science products for validating space-based rain estimates from the TRMM satellite. These products include gauge rain rates, and radar-estimated rain intensities, type, and accumulations, from four primary validation sites (Kwajalein Atoll, Republic of the Marshall Islands; Melbourne, Florida; Houston, Texas; and Darwin, Australia). Site descriptions of rain gauge networks and operational weather radar configurations are presented together with the unique processing methodologies employed within the Ground Validation System (GVS) software packages. Rainfall intensity estimates are derived using the Window Probability Matching Method (WPMM) and then integrated over specified time scales. Error statistics from both dependent and independent validation techniques show good agreement between gauge-measured and radar-estimated rainfall. A comparison of the NASA GV products and those developed independently by the University of Washington for a subset of data from the Kwajalein Atoll site also shows good agreement. A comparison of NASA GV rain intensities to satellite retrievals from the TRMM Microwave Imager (TMI), precipitation radar (PR), and Combined (COM) algorithms is presented, and it is shown that the GV and satellite estimates agree quite well over the open ocean.

1. Introduction

The Tropical Rainfall Measuring Mission (TRMM) is a satellite-based program to measure tropical rainfall and to help quantify the associated distribution and transport of latent heat, which drives the global atmospheric system. TRMM is a joint United States–Japan mission launched from Tanegashima, Japan, on 27 November 1997 (Simpson et al. 1996; Kummerow et al. 1998). TRMM has provided state-of-the-art precipitation measurements since shortly after launch and was boosted from its original 350-km orbit to a new orbit of 402.5 km in August 2001 in order to extend science observations beyond the original time frame of 2000. A key effort of TRMM has been dedicated to providing ground validation (GV) of the satellite rainfall estimates. The GV program is based in the TRMM Satellite Validation Office (TSVO) at the NASA Goddard Space Flight Center (GSFC) in Greenbelt, Maryland. The GV program has been collecting radar and rain gauge measurements since 1988 and continues to collect datasets at a number of sites located throughout the Tropics.

The aim of this paper is to provide a summary of GV operations, algorithm descriptions, and data quality. A description of the primary GV sites and details of their operational configurations, including a description of the network of radar and rain gauge networks at each site, are provided in section 2. Section 3 discusses the software system and algorithms developed and maintained by TSVO for processing the data, details data sources and ingest methodologies, and provides a brief description of the level I–III TRMM GV Science Products (TSP) and how they are produced. Section 4 provides a discussion on the error statistics of the radar rainfall estimates versus both dependent and independent gauge measurements, as well as a comparison of rain rates and monthly accumulations between TSVO and those produced by the University of Washington. Section 5 provides validation comparisons between TRMM GV and satellite-retrieved rain intensities generated by the TRMM Microwave Imager (TMI), precipitation radar (PR), and Combined (COM) algorithms.

Corresponding author address: David B. Wolff, NASA GSFC, Code 912.1, Greenbelt, MD 20771.
E-mail: wolff@radar.gsfc.nasa.gov

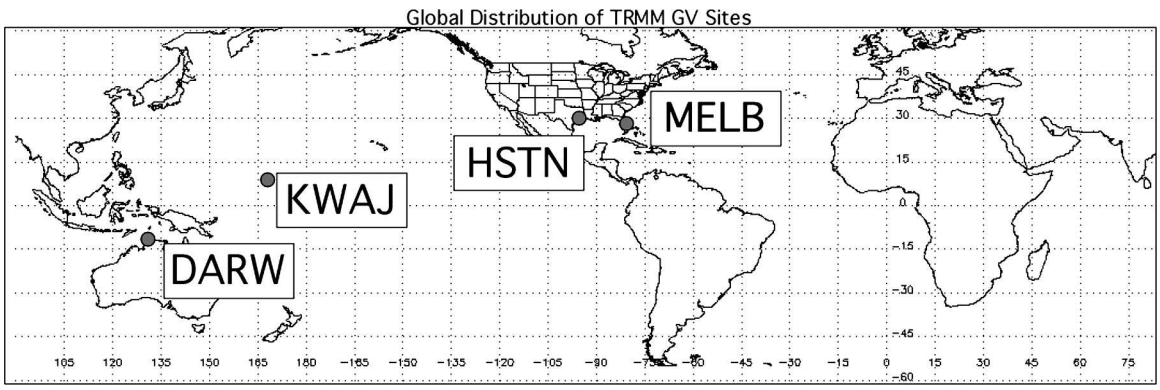

FIG. 1. Global map showing locations of the four TRMM GV sites: DARW (Darwin, Australia); HSTN (Houston, TX); KWAJ (Kwajalein, Republic of the Marshall Islands); and MELB (Melbourne, FL).

2. Description of current GV operations

The original plan for the GV Program selected 10 sites from various locations around the world for the purpose of climatological validation of the TRMM satellite precipitation estimates. Four of these sites were designated as Direct Data (DD) sites and six were designated as Direct Product (DP) sites. This paper focuses on the four selected DD sites: Kwajalein, Republic of the Marshall Islands; Melbourne, Florida; Houston, Texas; and Darwin, Australia. The global distribution of these sites is provided in Fig. 1. Figure 2 provides a 5-yr climatology of monthly rainfall totals derived from observed GV gauge data for the four DD sites. Figure 3 provides a 5-yr climatology of the diurnal cycle of occurrence of precipitation for the four DD sites, generated from observed GV gauge data. Details on the site-specific properties, Figs. 2 and 3, will be provided in the following sections describing the individual sites.

a. The GV network at Kwajalein

One of the primary goals of the TRMM mission is to validate satellite rain estimates over the open ocean with independent estimates obtained from regional surface sensors. A GV site was established on Kwajalein (KWAJ) Atoll in the Republic of the Marshall Islands, in the central Pacific Ocean. KWAJ is located on the northern edge of the Pacific intertropical convergence zone (ITCZ) and on the eastern boundary of the western Pacific warm pool. The atoll consists of a ring of small, flat coral islets, which are part of the vast archipelago scattered across the central Pacific. These islets have no significant orographic features and are thickly overgrown with palm trees and other tropical vegetation.

Figure 2 provides the mean monthly and annual rainfall for KWAJ (and the other GV sites). The annual rainfall at KWAJ is dominated by convective systems that form in the ITCZ. Most of the rainfall occurs in association with the northward migration of the ITCZ between April and October, which leads to a strong south-to-north gradient of annual rainfall. During the Northern Hemispheric winter, the ITCZ migrates farther to the south, producing a sharp (climatologically significant) increase in the trade winds. This increase is correlated with a decrease in total rainfall amounts and event frequency. Schumacher and Houze (2000) show that Kwajalein precipitation is also contributed to by a significant number of isolated, shallow (< 5 km) "warm rain" clouds.

Figure 3 shows the probability of occurrence of precipitation at each hour of the day (local time) and for

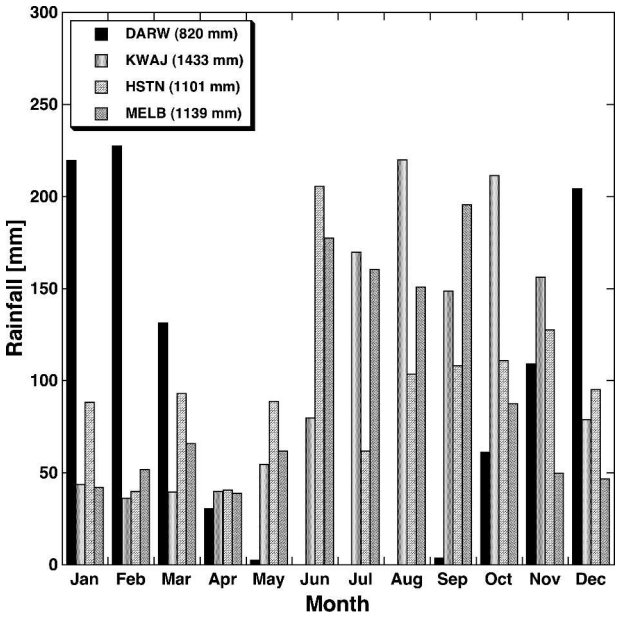

FIG. 2. Average mean monthly rainfall in mm for the four GV sites. These averages were computed using five years of available GV-sponsored gauge data from the period 1998–2002. The average annual rain accumulations are shown in parentheses in the plot legend. Note that these values may differ from the climatological mean, as they are derived from TRMM gauge data not climatological records.

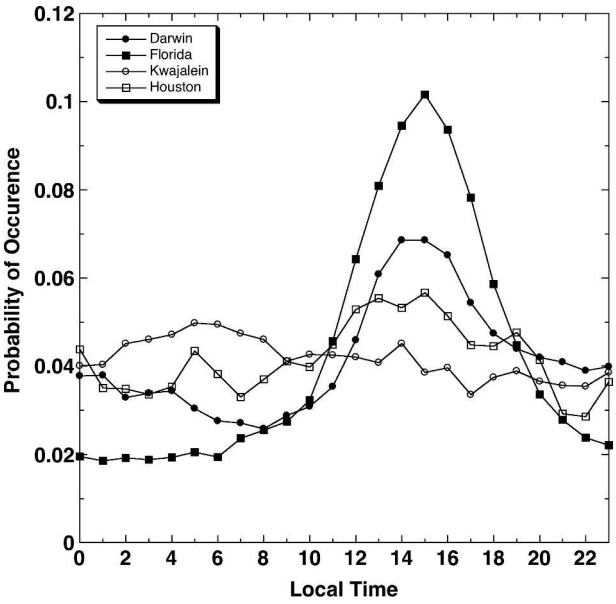

FIG. 3. Diurnal cycle of precipitation as expressed by the probability of occurrence of precipitation for a given hour (LT) at each of the four TRMM GV sites. These statistics were derived from five years of available GV-sponsored gauge data from the period 1998–2002.

KWAJ reveals a slight diurnal maximum between 0400 and 0600 LT; however, the amplitude is fairly weak, and convective showers can occur at any time of the day with about equal probability (Wolff et al. 1995). The diurnal cycle for KWAJ shown in Fig. 3 is consistent with other studies of diurnal rainfall over the open oceans, with the existence of a low-amplitude nocturnal maximum in rainfall associated with enhanced instability due to radiational cooling at the tops of clouds (Kraus 1963; Gray and Jacobson 1977; Hendon and Woodberry 1993).

Kwajalein Island is the command center for the Reagan Missile Testing Range of the U.S. Army at Kwajalein Atoll (USAKA), and weather operations conducted there primarily support military operations. The KWAJ radar is located on Kwajalein Island at 8.718°N, 167.733°W and is generally operated in a volume scan mode consistent with the scientific objectives of TRMM. The data are collected on Exabyte (8 mm) tapes and sent routinely to NASA GSFC. Kwajalein reflectivity data have a spatial resolution of 250 m for each 1° in azimuth. Table 1 provides the general characteristics of the KWAJ radar, also referred to as KPOL. Table 2 provides a description of the scanning strategy employed by KPOL.

TSVO operations at KWAJ are currently limited to small islets that extend from Kwajalein Island at the southern tip of the atoll to Roi Namur at the northern end. A map of the KWAJ GV radar and gauge network is provided in Fig. 4. The KWA gauge network of seven rain gauge sites (see Table 3) was first deployed in 1988

TABLE 1. Characteristics of the Kwajalein (KPOL) radar located on Kwajalein Island at the southern tip of Kwajalein Atoll in the Republic of the Marshall Islands.

Frequency range	2800 MHz
Peak power	700 kW at 58.5 dB
Normal power	500 kW
Pulse width	1.67×10^{-6} s
PRF intensity	264–1536 Hz
Radar range (maximum)	270 nm
Velocity	150 km (81 nm)
Antenna gain	43.8 dB
Antenna diameter	8.2 m (27 ft)
Antenna beamwidth	0.95°
Height to center of antenna	20.7 m (68 ft)
Input power	110/220 V single phase at 7.5–10.0 kW

in an early phase of the TRMM GV program. The locations of the KWA gauge network sites are labeled as squares on the map in Fig. 4. Current operations include two gauges at every site, but there are no gauge data available south of Kwajalein Island or north of Roi Namur, which is approximately 75 km from the radar.

b. Central Florida

Central Florida (MELB) was selected as another DD site for TRMM GV operations. The principal radar is located on the eastern Atlantic seaboard in Melbourne, Florida. The area observed by the radar is approximately 50% ocean and 50% land. Florida is a subtropical location that receives about 70% of its annual rainfall between June and September, as inferred from Fig. 2. Most of this rainfall is due to sea-breeze-induced isolated convective systems and large organized tropical storms. Florida's annual rainfall budget also receives a contribution from midlatitude synoptic systems during Northern Hemispheric winter months when frontal boundaries occasionally affect Florida weather.

The diurnal cycle of rainfall at MELB is highly periodic, being dominated by the frequent occurrence of sea-breeze-induced convection in the mid to late afternoon. The diurnal profile for MELB shown in Fig. 3 reveals a maximum in rain occurrence in the afternoon. In the summer months especially, this distinct climatological feature is connected with a periodic sea breeze/land breeze oscillation coupled to the diurnal heating cycle. According to Fig. 3, over 50% of the total rain occurs between 1200 and 1800 LT.

The MELB site is complemented by a Weather Surveillance Radar-1988 Doppler (WSR-88D) located at 28.113°N, 80.654°W. Figure 4 is a map of the MELB site that provides the location of the radar and the associated rain gauge networks. Crum et al. (1993) provide more information on the WSR-88D system and operations.

TSVO receives data from a broad distribution of gauges spread across the MELB GV site, as shown in Fig. 5. Although the gauge sampling is quite good over-

TABLE 2. Task configuration for KPOL radar. Columns are task name, radar polarization, azimuth sweep rate (deg s^{-1}), elevation angles (deg), pulse repetition frequency, and run time (min: s).

Task	Polarization	Rate	Elevation angles	PRF	Time
Surv_TRMM	Horizontal	8	1.0	396	00:53
GVVOL_A	Dual	15	0.4, 2.3, 4.2, 6.1, 8.0, 9.9, 11.8, 14.0, 16.6, 19.6, 23.2, 27.6	960	05:25
GVVOL_B	Dual	15	0.4, 1.4, 3.3, 5.2, 7.1, 9.0, 10.9, 12,9, 15.2, 18.0, 21.3, 25.3	960	05:25

all, the gauge density is variable from sector to sector and no coverage exists in the far western sector of the state at a distance greater than 100 km from the radar, or over the Atlantic Ocean. Four separate networks provide data for GV efforts: Kennedy Space Flight Center (KSC), St. Johns Water Management District (STJ), South Florida Water Management District (SFL), and an 18-gauge (over a 48-km^2 area) dense-scale network at the Triple-N ranch (NNN). The KSC and NNN networks are owned and operated by NASA. The STJ and SFL networks are operated by their Florida Water Management districts. The number of gauges in each of these networks is shown in Table 3. Data is processed by TSVO on a month-to-month basis and special arrangements have been made with the site managers of each network for timely, routine transfer of the data to NASA GSFC.

c. Southeast Texas

The southeast Texas GV network (HSTN) is shown in Fig. 6. This site provides observational coverage for the coastal regions of Texas and western Louisiana and a large inland region north and west of Houston and also extends southward approximately 100 km into the Gulf of Mexico. The mean precipitation for the Houston area averages about 1200 mm yr^{-1}. Figure 2 does not suggest a strong mean seasonal cycle of monthly rainfall, but some variability is observed, with a maximum monthly rainfall observed in June (~205 mm). Regionally, however, there is a strong geographical west-to-east gradient in annual average precipitation, ranging from 600 mm yr^{-1} in the west to over 1500 mm yr^{-1} in the east. The mean diurnal cycle in Fig. 3 shows a relatively weak afternoon maximum with only slight variation in the probability of precipitation as a function of the time of day. Florida and Darwin, for instance, show stronger afternoon amplitude, suggestive of a more active convective heating cycle.

The primary radar for the Houston site is the WSR-88D located in League City, Texas, at 29.472°N, 95.079°W. This radar has characteristics similar to the WSR-88D radar at MELB (Crum et al. 1993). Figure 6 provides a regional map of the Houston area, showing the radar and gauge locations. The gauges are maintained and operated by the Harris County Emergency Operations Center. As indicated in Fig. 6, most of the gauges are distributed around Harris County, Texas, and around an axis extending about 100 km northwest of the radar. Consequently, the spatial sampling inferred from the density distribution of gauges varies markedly, with only a few gauges located near the coast and south of the radar. It should also be noted in Table 3 that the bucket size is 1.0 mm, four times larger than the standard 0.254 mm of the other GV networks, excluding Darwin, which is 0.2 mm. The bucket size is

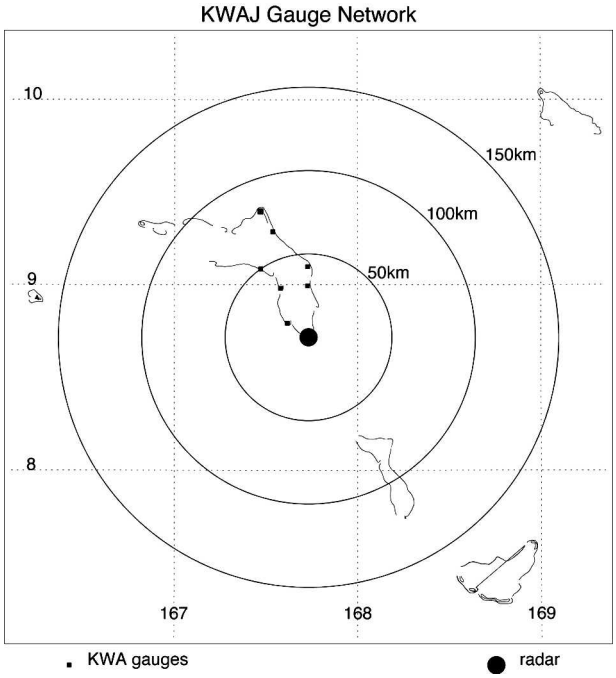

FIG. 4. Map of the KWAJ radar and gauge network. Gauge locations are shown as black triangles. The KPOL S-band radar is located on Kwajalein Island at the center of the figure

TABLE 3. Description of the available networks, number of locations, gauge types, and tipping-bucket rain increment for the four TRMM GV sites.

GV site	Gauge network	No. of gauge sites	Rain increment (mm)
Kwajalein	Kwajalein	7	0.254
Melbourne	St. Johns WMD	27	0.254
	NASA Kennedy Space Center	33	0.254
	South Florida WMD	129	0.254
	Triple-N Ranch	20	0.254
Houston	Harris County	165	1.000
Darwin	Darwin C-Scale	33	0.200

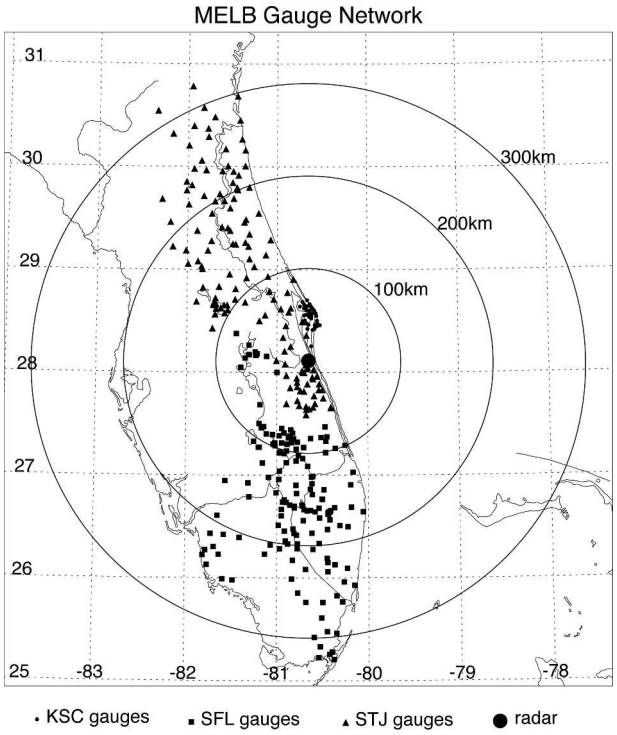

FIG. 5. Map of the three rain gauge networks (KSC: Kennedy Space Center; SFL: South Florida Water Management District; and STJ: St. John's River Water Management District) deployed at the Melbourne, FL, TRMM GV site. The three networks are denoted as circles, squares, and triangles, respectively. KSC network gauges are located on Cape Canaveral, approximately 50 km northeast of the KMLB WSR-88D radar (center). A Dense Rain Gauge Network (DRGN, not shown) is located approximately 40 km west of the radar.

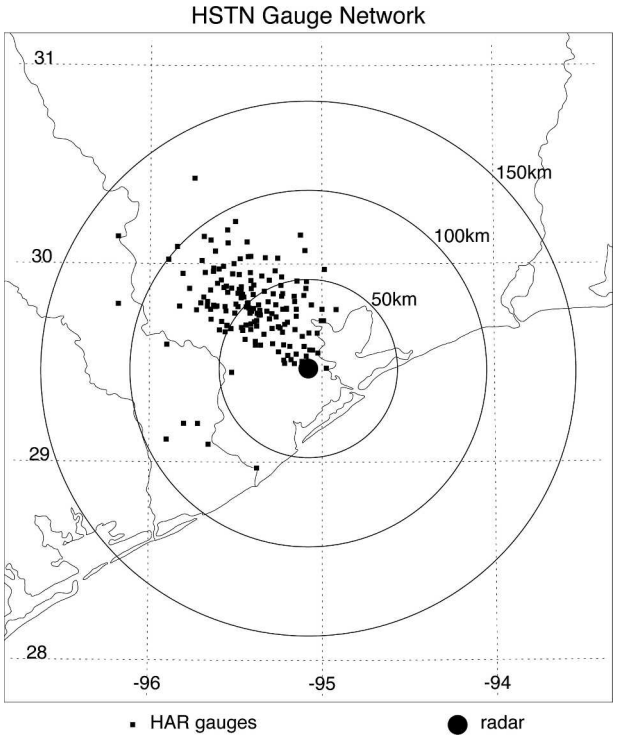

FIG. 6. Map of the Harris County (HAR) rain gauge network deployed at the Houston TRMM GV site. Most HAR gauges are located to the northwest of the KHGX WSR-88D radar (center).

important in the determination of rain rates inferred from the discrete time series of tips. The larger bucket size effectively reduces the time resolution of the rain rates in each rain event, as fewer tips are collected over a characteristically longer period, limiting the ability to calculate light rain rates.

d. Darwin, Australia

Darwin, Australia (DARW), is located on the north-central coast of Australia and borders the southern edge of the Indonesian Maritime Continent. The radar coverage also includes Melville and Bathurst Islands, which exert a strong effect on the regional rainfall climatology. The annual cycle at Darwin is distinctly bimodal, characterized by wet and dry seasons (Fig. 2). The "rainy" season extends from November to April and accounts for over 90% of the annual rainfall. Keenan and Carbone (1992) classify two primary rain regimes around DARW during the rainy season: monsoon and break periods. Monsoonal periods are associated with a westerly maritime flow regime characterized by weak convection but widespread regional coverage. Monsoonal pulses typically last less than a month and occur about three times in a given rainy season. Break periods are identified with an easterly continental flow regime characterized by deep convection in association with large organized propagating squall lines and smaller isolated convective systems. Some of the deepest convection in the world occurs over Melville and Bathurst Islands, about 50 km off the northern coast. Thunderstorms are observed over these islands 65% of the days during the break periods (Keenan and Carbone 1992). The diurnal cycle at DARW is highly variable and, to a large extent, regime dependent. Figure 3 shows a large maximum in the occurrence of precipitation in the afternoon and early evening hours. Much of this precipitation is contributed to by the massive thunderstorms that develop via sea breeze convergence over the islands, and sea breeze and air mass convection over the mainland as well as nocturnal squall lines and widespread monsoonal rainfall.

The Darwin radar is located at 12.248°S, 130.925°E and is operated and maintained by the Australian Bureau of Meteorology Research Center (BMRC). The radar is operated only during the Southern Hemisphere summer (November–March) each year and generally in a surveillance mode of 15–30-min volume scans and periodic base scans (low level only). During special observing periods (SOPs), the radar is operated in an enhanced mode with 5–15-min volume scans and 5-min base scans.

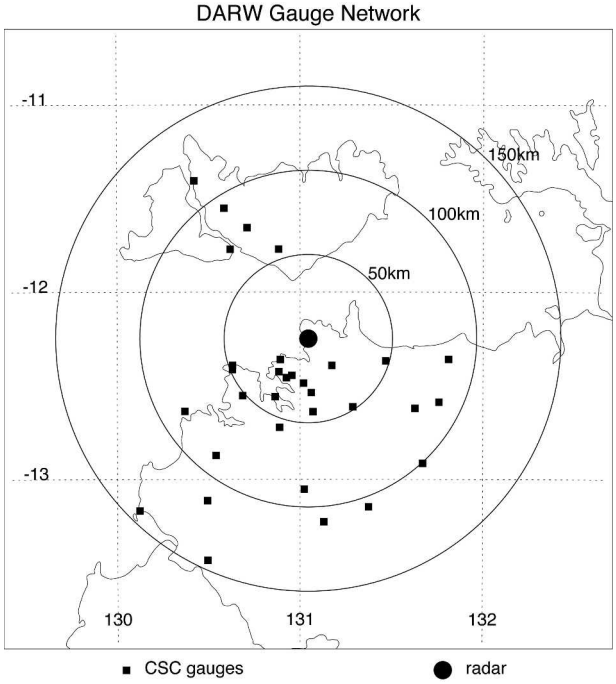

FIG. 7. Map of the CSC rain gauge network deployed at the Darwin TRMM GV site. Other higher-scale networks are available but not shown. The Darwin C-band polarimetric (C-POL) radar is located at the center of the figure.

Data from the Darwin (C-POL) radar are recorded with a variable spatial resolution ranging from 250 m to 1 km for every 1° in azimuth (Keenan et al. 1998).

The DARW gauge network is shown in Fig. 7. This gauge network provides regional coverage over land, though the gauges on west Melville Island dominate sampling over the islands. There are also a few higher-resolution networks located to the southeast of the radar (not shown) that provide additional information on the scale-related variability of precipitation near Darwin and can be used for validation the radar rainfall estimates.

3. Ground validation science data products

In order for the TSVO to produce the myriad of products specified by the TRMM Science Team, a rather extensive package of programs and libraries was developed. The principal libraries are the Radar Software Library (RSL) and the Ground Validation System (GVS). These packages are available under the GNU Public License and can be obtained from the TRMM Office Web server. RSL supports a number of different ingest formats, including Universal Format (UF), SIGMET®, and WSR-88D Archive II. RSL also supports output in UF and Hierarchical Data Format (HDF). (Further information on RSL can be found online at http://trmmfc.gsfc.nasa.gov/trmm_gv/software/rsl/index.html.)

Figure 8 depicts the basic level I and level II processing flow of TRMM GV radar data. Data from MELB and HSTN are now received in near real time over the Internet via an arrangement with the WSR-88D Operational Support Facility (OSF), the National Climatic Data Center (NCDC), and the National Weather Service (NWS). Radar data from the other primary sites are collected on 8-mm tapes and sent directly to GSFC. Data from Kwajalein usually arrive on a biweekly basis. Darwin data is received in two or three batches throughout the rainy season. Radar data are collected from the Houston, Melbourne, and Kwajalein sites on a year-round basis, while Darwin data are collected only during the rainy season (November–April).

Radar data are processed into two standard TRMM GV level I products using the GVS software package (Marks et al. 2000; Kulie et al. 1999). Two primary level I processing tasks are performed, converting radar data into a common format for archival, and quality control (QC) of the reflectivity data. Level I products are in polar coordinates and are written in HDF to conform to official archival standards of the DAAC. For brevity, Table 4 provides a description of the TSP for levels I, II, and III. Details on the more important aspects of their generation, specifically the means by which the radar rainfall estimates are produced, are discussed in the following section. Marks et al. (2000) provide more extensive detail on the available GV products.

4. Radar rainfall estimation

Many researchers have addressed the issue of rainfall estimation from radar. Summaries can be found, for example, in Wilson and Brandes (1979), Doviak (1983), Austin (1987), Atlas (1987), and, more recently, Atlas et al. (1997). The approach adopted by the TRMM GV program at NASA GSFC is to use operational rain gauge networks and ground-based radar data to derive Z_e–R relationships and precipitation estimates. An integral part of this process is the evaluation of product quality or the degree of confidence we have in the accuracy of the estimates. Rain gauges serve a key function in capturing point measurements of surface rainfall. Networks of gauges with broad spatial distributions allow the best opportunity for meaningful comparison with ground-based radar.

Rain gauges are precision instruments that need to be adequately calibrated in the laboratory prior to deployment in the field and at regular intervals thereafter. Rain gauges are also subject to the elements and suffer complications due to typical weathering in the harsh tropical environments in which they are deployed. Data dropouts related to short-duration glitches or longer-term failures of onboard loggers can and do occur. A description of sampling errors of tipping-bucket rain gauge measurements can be found in Habib et al. (2001) and Ciach et al. (1997). A persuasive argument can be made for a system of densely spaced gauges to provide sufficient spatial coverage as well as multiple gauges at each individual location to provide redun-

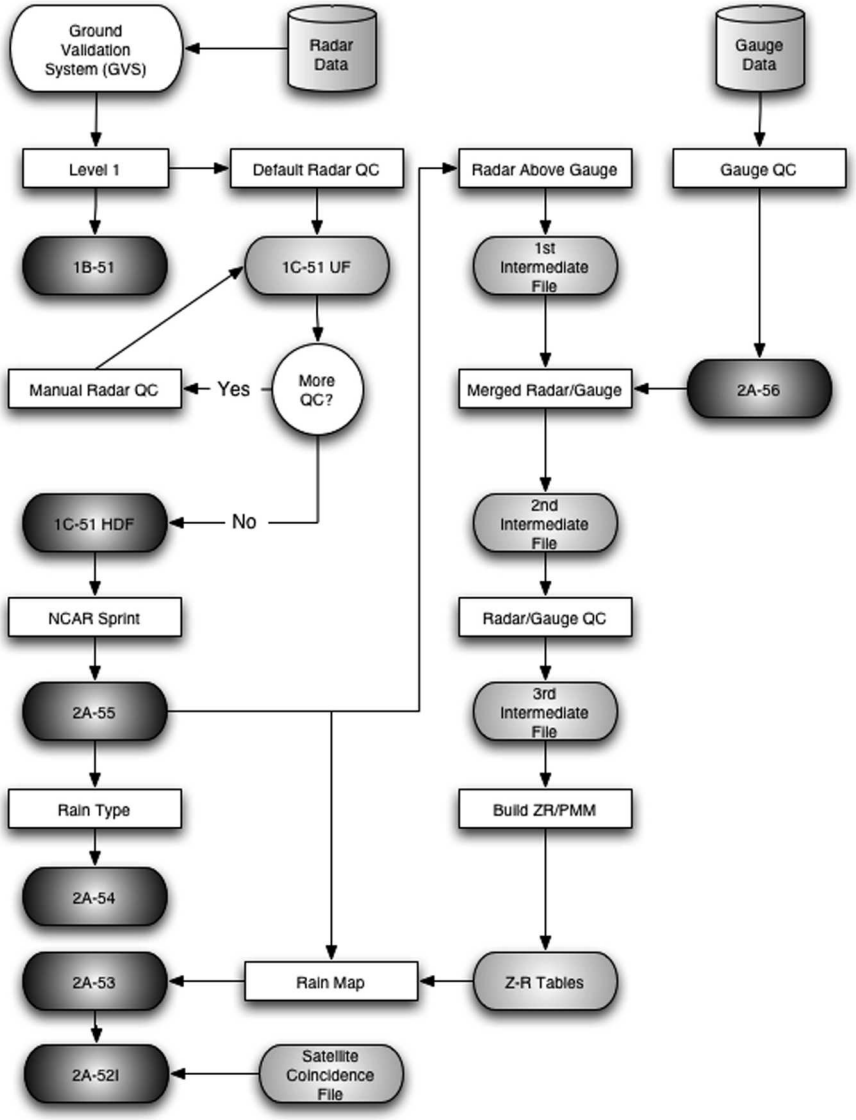

FIG. 8. Flowchart of TRMM GV data processing, quality control, and product generation. TRMM Standard Products (TSP) are indicated by darkened ovals and are defined in the text. Algorithms or programs are represented by rectangles, and lighter ovals represent intermediate files created in the Z_e–R table generation.

dancy and to mitigate the impact of mechanical breakdown on data collection efforts.

a. Data extraction and merging for Z_e–R development

Official GV rainfall products are developed in modular steps with distinct intermediate products. These developmental steps include 1) extracting quality-controlled radar data over the locations of rain gauges, 2) merging gauge and radar data in time and space, 3) automated quality control of radar and gauge merged data, and 4) deriving Z_e–R lookup tables for converting observed radar reflectivities into rain intensities from the merged data.

In the first step, reflectivity data from the 2A-55 product is extracted over validation rain gauge locations. Data from the 1.5- and 3.0-km Constant Altitude Plan Position Indicator (CAPPI) levels are extracted from each radar volume scan (over the course of one month) from the pixel over rain gauge locations. Each radar pixel size is 2 km $\times$ 2 km and the extracted gauge data is from the 7 min centered at the radar volume scan time, as explained in more detail by Amitai (2000).

The rain gauge data are then merged in time and space with the extracted reflectivities to create a second intermediate (merged) file for Z_e–R development. Up to this point, independent QC techniques have been applied to both the radar and rain gauge data. An au-

TABLE 4. Description of the primary TRMM Standard Products produced for the Ground Validation Program.

Product	Fields	Description
1B-51	DZ, VR, ZDR	Original coordinates and fields. Maximum range 230 km.
1C-51	CZ, DZ, VR	Original coordinates. CZ contains quality-controlled DZ field. Maximum range 200 km. HDF format.
2A-52	Echo coverage	Percentage echo coverage with satellite coincidence. ASCII format.
2A-53	R	Cartesian grid (2 km × 2 km, 151 × 151 pixels). Instantaneous rain intensity (mm h^{-1}). Maximum range 150 km. HDF format.
2A-54	Rain type	Cartesian grid (2 km × 2 km, 151 × 151 pixels). Rain type (stratiform or convective). Maximum range 150 km. HDF format. From Steiner et al. (1995).
2A-55	CZ	3D Cartesian grid (2 km × 2 km horizontal, 1.5-km vertical; 151 × 151 × 13 pixels). Quality-controlled reflectivity. Maximum range 150 km. Maximum height 19.5 km. HDF format.
2A-56	R	1-min average gauge rain rates. One file per month, per gauge. ASCII format.
3A-53	R	Cartesian grid (2 km × 2 km). Five-day integrated rainfall. Maximum range 150 km. HDF format.
3A-54	R	Cartesian grid (2 km × 2 km). Monthly integrated rainfall. Maximum range 150 km. HDF format.
3A-55	R	3D monthly structure with vertical profiles. HDF format.

tomated QC algorithm (Amitai 2000) is applied to the combined radar and rain gauge data to determine which rain gauges (on a monthly scale) are unreliable for the purposes of Z_e–R development. The reliability of a particular rain gauge is determined upon comparison with the associated radar data above the gauge location. When a gauge is considered unreliable for a particular month, all data from both the gauge and extracted radar pixels above that gauge are filtered from the merged file. This procedure ensures that only objectively determined "good" gauges are used in the monthly Window Probability Matching Method (WPMM) Z_e–R development. WPMM matches the probabilities of radar-observed reflectivities Z_e and gauge-measured rain intensity R in such a way that the probability density function (PDF) of the radar-estimated R above the gauge will be identical to the PDF of the gauge rates on a monthly scale. The resulting Z_e–R functions are found to be curved lines in log–log space rather than a straight-line power law (Rosenfeld et al. 1994).

Moreover, the PDF of the gauge rates was found to better represent the true PDF of R at the scale of a radar pixel than the one based on application of a gauge-adjusted power Z–R relationship (Amitai et al. 2004). Therefore, the application of the WPMM Z_e–R relationships will allow better evaluation of the instantaneous rainfall based on comparing the satellite-based PDF of R with PDF derived from coincident ground observations (Amitai et al. 2005).

b. Site-specific considerations and challenges

Due to the inherent characteristics of the available GV networks, owing mostly to geography and logistical realities, different techniques for deriving the Z_e–R relationships must be employed.

At MELB, monthly unconditional distributions of Z_e and R from the QC merged data are used to derive specific month-to-month Z_e–R lookup tables. The Melbourne WSR-88D radar is stable and well calibrated, which allows the WPMM technique to be applied on a month-to-month basis (Anagnostou et al. 2001). To mitigate range effects on the results (Rosenfeld et al. 1992), multiple-range (15–50, 50–98, and 98–150 km) Z_e–R relationships are used. There are three rain gauge networks with gauges distributed throughout all ranges (see Fig. 5). For a given month, each range has its own uniquely determined WPMM Z_e–R lookup table based on the unconditional distributions of Z_e and R found within that range. The Z_e distributions are obtained by extracting reflectivity from specific CAPPI heights directly over gauge locations. For the closest ranges (15–50 and 50–98 km), NCAR Sorted Position Radar Interpolation (SPRINT) interpolated reflectivities are extracted from the 1.5-km CAPPI height over validation gauge locations. For the outer range (98–150 km), the interpolated reflectivities are extracted from the 3.0-km CAPPI height over validation gauge locations. Resulting WPMM Z_e–R lookup tables are then applied directly to the same CAPPI levels from which they were derived to obtain instantaneous rain-rate map products (TSP 2A-53). There is no distinction between convective and stratiform classifications in Z_e–R development.

Monthly rainfall accumulation products (TSP 3A-54) are obtained by integrating the instantaneous rain rate maps over time. Integration parameters are defined by the time difference ΔT between successive radar volume scans. This scheme assumes that instantaneous rain rates remain constant for the duration of the specific radar scan up to a maximum ΔT of 10 min. When ΔT exceeds 10 min, the rain rate map immediately following the data gap is integrated for 5 min. The 5-min period was chosen as it represents the approximate time required to complete the WSR-88D volume

scan. This integration scheme is applied to all radar volume scans for each month at the Melbourne, Florida, validation site.

At KWAJ, the lack of "good" gauge data provides unique circumstances that require different techniques than those employed at MELB. For KWAJ, monthly WPMM Z_e–R development is not performed due to the limited number of rain gauge sites. On average, data from less than seven good gauges are available each month. To circumvent this problem and to create adequate Z_e and R distributions, quality-controlled radar and gauge merged data from the entire year of 2002 were combined. This large-scale data compilation procedure captures a full spectrum of precipitation events and provides robust distributions for WPMM Z_e–R development. Because most of the good gauges are within 98 km of the Kwajalein S-band polarimetric radar, we take a special approach to the Z_e–R development. SPRINT-interpolated reflectivity data are extracted over the gauge locations from both the 1.5- and 3.0-km CAPPI levels. Data from the 1.5-km (3.0-km) level are used in the Z_e distribution to develop a Z_e–R lookup table for the 15–98 km (98–150 km) range. By this technique, we are assuming that the Z_e–R distributions obtained from radar and gauges within 98 km can be used to develop Z_e–R lookup tables that are applied to the areas both inside and outside 98 km. The monthly rainfall accumulation scheme employed at KWAJ is very similar to MELB in that the instantaneous rain rate maps are integrated over the time difference ΔT between successive radar volume scans. The maximum ΔT for integration is 15 min. If ΔT exceeds 15 min, the rain rates from the instantaneous map immediately following the gap are integrated for 10 min. The 10-min period was chosen as it represents the approximate time between successive volume scans (with the current scanning strategy).

The calibration of the KWAJ radar has been a problem for the duration of the mission. There are currently few opportunities to determine, post hoc, the calibration of the radar at any given period due to poor record keeping and numerous hardware failures. Based on our use of the 2002 baseline KWAJ calibration, we are able to detect periods during which the relative calibration differed from the baseline and are working to determine methodologies to apply these corrections for future versions. Although the KPOL radar is dual-polarized, past quality of the data has been too poor to use for determining the absolute calibration, although we believe recent improvements to the radar may make use of data feasible for such purposes for current and future data. For past data, we are currently investigating other techniques to provide unbiased estimates using the clutter detected during periods when there is little or no precipitation present. In 2002, the radar appears to have been relatively stable and without significant hardware and known calibration issues. For this reason, 2002 was selected for the WPMM yearly technique. It is noted that, although the radar system appeared to be stable for this period, an absolute calibration offset might still need to be applied. Radar calibration fluctuations introduce a significant source of error into both instantaneous and monthly rain maps. The TRMM GV group is working to quantify and apply calibration offsets in such a manner that still allows independent evaluation/validation of TRMM satellite retrievals. One technique being considered is the application of a monthly radar- and gauge-determined bulk-adjustment factor. The bulk-adjustment factor would shift the entire WPMM curve in log–log space without altering the slope and would calibrate the Z_e distribution to match R from the gauges. This method, of course, could not be used if there are no good gauges for a particular month. By using the 2002-based WPMM, we were able to detect periods during which the relative radar calibration was different than the 2002 baseline.

c. Dependent versus independent validation

To evaluate the monthly rainfall product over a given site, several different validation methods (dependent, quasi-independent, and independent) have been employed. In the dependent validation process, rain gauge data that were used to create the R distribution for the monthly WPMM Z_e–R are compared with radar rain-rate accumulations. The resulting statistics from dependent validation are basically an algorithm and technique sanity check. Figure 9 shows an example of dependent validation results at MELB for August 1998. Quality-controlled rain gauge data (TSP 2A-56), which we assume to be the ground truth estimate of surface rainfall, are shown on the abscissa. Dependent validation (by definition) will result in a radar-to-gauge (R/G) ratio very close to unity (Table 5). For quasi-independent validation, if the number of gauges in a network is sufficient, a given percentage of the gauges can be randomly selected and isolated from the total set of gauges and then not used in the generation of the R distribution. We refer to this as a *quasi-independent* validation, as the initial set of data has been altered to a slight degree. In an independent validation, an entirely separate network of gauges exists for validation. In this case, the original data collection network remains intact. In the TRMM era, these conditions were met only over the MELB site during the second Texas–Florida Underflights Experiment (TEFLUN-B) conducted in the summer of 1998. Independent validation was conducted by the TRMM GV group (also Habib and Krajewski 2002) from TEFLUN-B. The existence of independent gauge networks for validation is an essential factor in the generation of dependable rainfall estimates.

d. Selecting and using independent gauges for validation

For MELB, August 1998 was a unique month in that a true independent validation of the TSP 3A-54 was

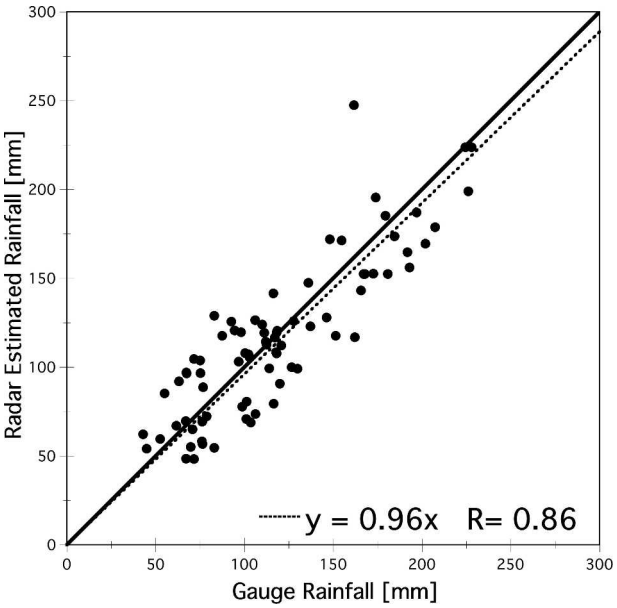

FIG. 9. Evaluation of Aug 1998 monthly rain accumulations against dependent rain gauge data (i.e., gauge data shown were used in the development of the applied monthly WPMM Z_e–R lookup tables) from the Melbourne GV site. Each symbol represents a monthly accumulation (mm) from the rain gauge (2A-56) and radar estimate above the gauge (3A-54).

possible. Independent validation of this specific monthly rain map is accomplished by validating against gauge data that were not used in Z_e–R development. The August 1998 results (Fig. 10) are based on data from 15 independent gauges that were installed in the Melbourne vicinity for the TEFLUN-B TRMM field campaign. These 15 gauges were not used in the operational WPMM Z_e–R development. Table 5 shows an R/G bias of 1.08, or an 8% overestimation by the radar, and normalized mean absolute difference (MAD) of 0.09 for these data. The MAD is defined as the mean of the absolute differences between monthly gauge and radar accumulations. These monthly statistics fall within acceptable bounds and are consistent with the independent findings of Habib and Krajewski (2002). Amitai et al. (2001, 2002) point out that such a low MAD might be explained by the natural variability of rain and gauge instrumental errors, and, based on further analysis of the same dataset as in Fig. 10, they demonstrated (see their Fig. 1) that the difference in accumulations of the gauges located within the same radar pixel were of the same order as the MAD, suggesting that the radar accuracy may be higher, but a denser gauge network is required for verification.

True independent gauge data are not available every month or at every site, so a technique was devised for quasi-independent evaluation. Quasi-independent gauge data are obtained by withholding 10% of the dependent gauges from a particular month from the WPMM Z_e–R process. Gauges to be withheld are selected using a random number generator based on atmospheric noise (available online at http://random.org). New Z_e–R lookup tables are developed and applied without these randomly selected gauges. The resulting monthly rainfall accumulation map is then compared directly with these withheld gauges. Technically, this method does not evaluate the official monthly rainfall product; however, due to the small percentage of gauges withheld, significant changes to the Z_e–R distributions have not been noted.

Figure 11 shows the dependent validation from MELB for September 1998, and Fig. 12 shows the quasi-independent validation results for that month. The dependent validation (Table 5) lists a R/G ratio of 1.01 (as expected), and a MAD of 0.14. Quasi-independent results using eight randomly withheld gauges from Z_e–R development (Fig. 12), show a R/G ratio of 0.93 and MAD of 0.12. Table 6 provides a 16-month summary of quasi-independent validation results from MELB. Relatively rainy months were chosen. The 16-month radar-to-gauge bias is 1.004. MAD values range from 0.08 to 0.28. As explained in Amitai et al. (2001), the natural variability of rain (within the scale of a radar pixel) and gauge instrument errors may explain a major fraction of the MAD. Point measurements from gauges are not at the same scale of a radar pixel, so gauge-based PDFs of R, which are used as ground truth, may not be representative of the actual R distribution at the scale of a radar pixel (Amitai et al. 2002). It is difficult to address this issue, as sufficiently

TABLE 5. Results of ground validation comparisons between gauge-measured monthly rainfall and those of WPMM radar estimates. There are three types of validation (VT): 1) fully independent (IND), in which gauges that are used for validation are not used for determination of the WPMM probabilities; 2) dependent (DEP), in which gauges that are used for determination of the calibration are also used for validation; and 3) quasi-independent (QUA), in which a subset of the total number of gauges are excluded in the determination of the WPMM probabilities, but then are used for validation (see text for further details). Also shown are the periods over which the validations are made, the mean rainfall of the gauges and radar estimates, as well as the bias, relative to the gauge mean, expressed in percent, and the MAD, defined as the mean absolute difference between the gauge and radar rain totals.

Site	VT	Period (yr/mo)	Gauge mean	Radar mean	R/G ratio	Bias (%)	MAD
MELB	DEP	1998/08	180.47	179.10	0.99	+1.0	0.16
MELB	IND	1998/08	135.08	145.23	1.08	−7.5	0.09
MELB	DEP	1998/09	111.55	112.50	1.01	−1.0	0.14
MELB	QUA	1998/09	190.01	177.63	0.93	+6.5	0.12
KWAJ	IND	1997–2001	180.92	166.92	0.92	+7.7	0.18

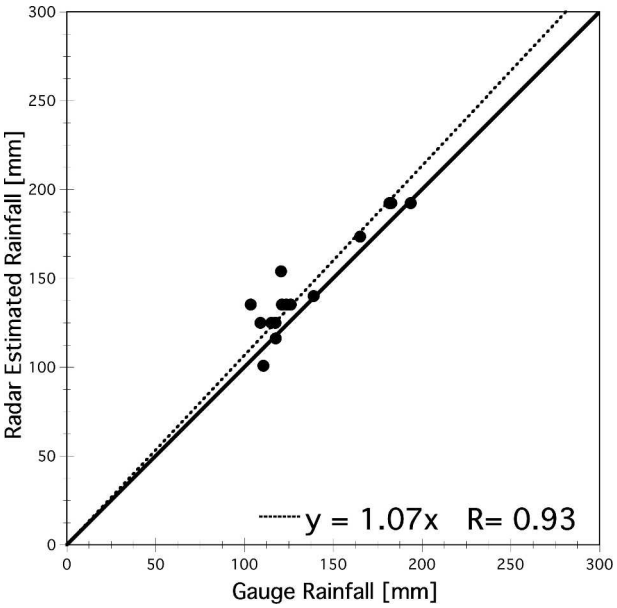

FIG. 10. As in Fig. 9 except that the gauges plotted were not used in determination of the Z_e–R algorithm and thus provide independent validation of the radar estimates.

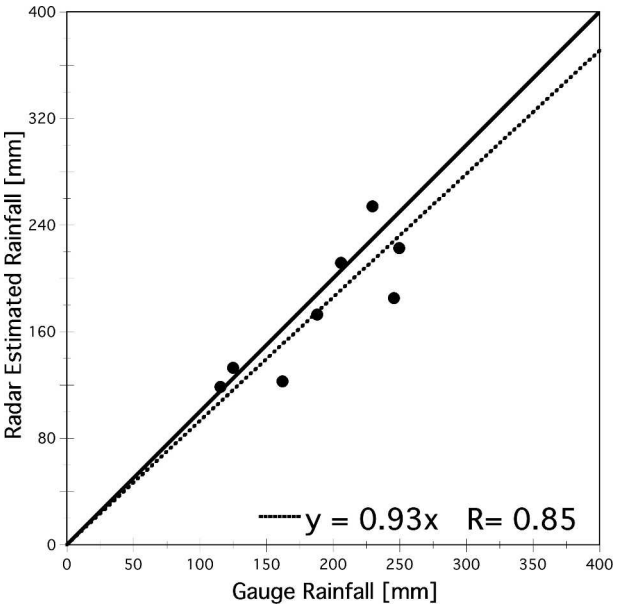

FIG. 12. As in Fig. 9 except for quasi-independent gauges (i.e., subsets of gauges are removed from the population of regular gauges prior to development of the Z_e–R relations).

dense gauge networks necessary to represent the distribution of R at a radar pixel size are not available at TRMM GV sites. It may be feasible to apply this quasi-independent validation approach to additional validation sites, such as Houston and Darwin, and potentially new GV sites such as the Florida Keys (Wolff et al. 2003), and Wallops Island, Virginia. However, the quasi-independent validation approach just described should not be applied to the Kwajalein Atoll site due to the limited amount of good rain gauge data.

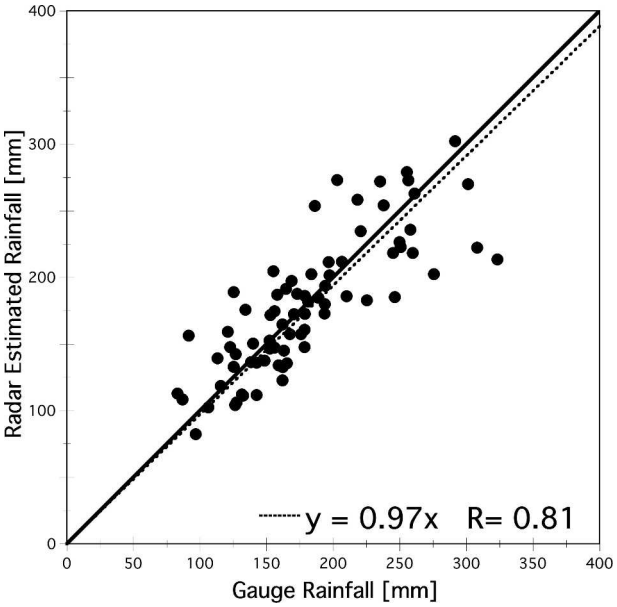

FIG. 11. As in Fig. 9 except that the period of coverage is for Sep 1998.

As was previously mentioned, the entire year of radar and rain gauge data from 2002 (except December) was used in developing the KWAJ Z_e and R distributions for a yearly based WPMM Z_e–R to be applied to all months. Therefore, any gauges considered "good" from months other than from year 2002 can be considered independent and used for validation purposes. From December 1997 through December 2001, only 18 months out of a possible 49 months had statistics within acceptable bounds for reliable rainfall estimation and validation. Acceptable statistical bounds are subjectively defined in this study as follows: MAD < 0.3, and R/G ratio between 0.75 and 1.25. From these 18 months, R/G ratios ranged from 0.79 to 1.19, while the MAD varied from 0.11 to 0.27. For the dependent months (January–November 2002), R/G ratios varied from 0.79 to 1.23, while the MAD varied from 0.12 to 0.25. Figure 13 shows an ensemble scatterplot with the combined results of the 18 months with acceptable radar and gauge comparison statistics. All gauges used in this plot are considered independent. Additional scatterplots and validation statistics are posted on the TSVO Web site (http://trmm-fc.gsfc.nasa.gov/trmm_gv).

e. Comparison of rain estimates at KWAJ

Both the TSVO and the Department of Atmospheric Sciences at the University of Washington (UWASH) have produced TRMM GV products at KWAJ. The

TABLE 6. Quasi-independent monthly validation for Melbourne, Florida. Shown are the month and year, radar-to-gauge ratio, mean absolute deviation, and the number of gauges that were used to derive the statistics.

Date	R/G ratio	MAD	No. of gauges
Nov 1998	0.94	0.08	6
May 1999	1.02	0.19	9
Jun 1999	0.95	0.17	10
Aug 1999	1.00	0.16	9
Sep 1999	1.10	0.21	9
Oct 1999	1.08	0.10	9
Jul 2000	0.94	0.25	10
Sep 2000	0.92	0.28	10
Jun 2001	1.12	0.20	10
Jul 2001	1.07	0.21	10
Aug 2001	0.97	0.14	10
Sep 2001	0.96	0.10	10
Jun 2002	1.05	0.11	9
Jul 2002	0.90	0.23	11
Aug 2002	0.95	0.20	10
Dec 2002	1.04	0.09	7

methodologies used to produce these estimates vary slightly, but overall the results compare quite favorably with one another. The UWASH group uses a disdrometer-based Z–R to convert radar reflectivities into rain intensities. A description of their methodology is provided in Houze et al. (2004, manuscript submitted to *J. Appl. Meteor.*).

Here we will present a comparison of Level II (rain intensity) and Level III (monthly rainfall) for the

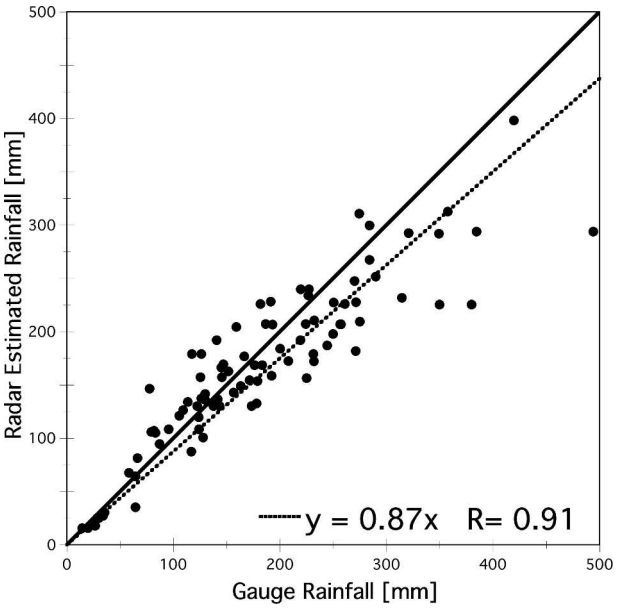

FIG. 13. Sixteen-month ensemble validation results from the Kwajalein Atoll GV site. The WPMM Z_e–R lookup table was derived from 2002 data (see text); therefore, gauge data from years other than 2002 are being considered independent. The 16-month period (which resulted in 90 radar and gauge plotting points) is from data prior to year 2002.

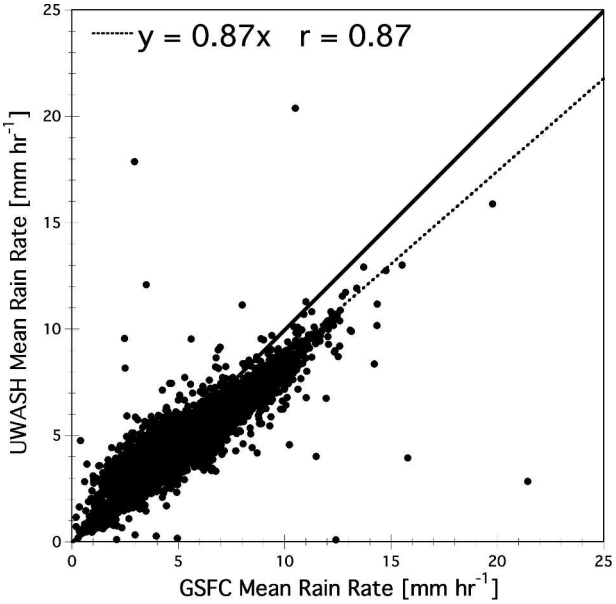

FIG. 14. Scatterplot illustrating a comparison between TSVO and UWASH mean rain rates for the KWAJ radar. Each point represents the mean rate of a given instantaneous rain map from the two products. There are approximately 144 rain maps observed each day, and the plot shown covers all such rain maps produced for the period 1 Jul–31 Dec 1999. Also shown is the regression equation between the two estimates as well as their correlation.

TSVO and UWASH products. The purpose of this effort is to provide the community with an understanding of the relative magnitudes of rainfall over KWAJ, as well as to provide an estimate of the relative difference between the two approaches.

f. Level II comparisons

The GV data from July through December 1999 were selected for comparison, based on the current availability of the UWASH products. This dataset provided approximately 4500 rain intensity maps for comparison. Only time-coincident maps were compared. For each map, the conditional mean rain rate was computed; that is, only points that were nonzero in both products were considered. Figure 14 provides scatterplots of these mean rain map values for each month. The two rain intensity estimates are well correlated ($r = 0.87$). TSVO rain intensities average about 13% higher than the UWASH estimates over the period.

g. Level III comparisons

For the level III comparisons, the six monthly rainfall maps (TSP 3A-54 and 3A-54UW) were used. The conditional mean rain rate was computed for each map, and Fig. 15 provides a comparison between the TSVO and UWASH level III estimates. The monthly rainfall estimates are perfectly correlated, but the TSVO esti-

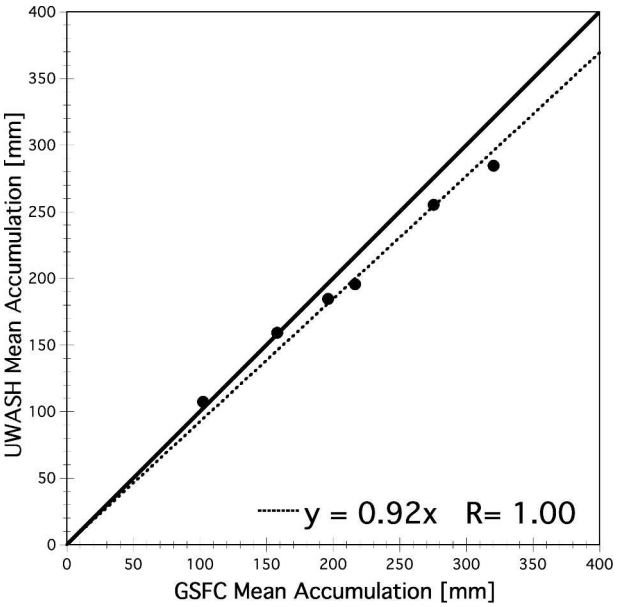

FIG. 15. Scatterplot illustrating a comparison between TSVO and UWASH mean monthly rainfall for the KWAJ radar. Each point represents the mean rate of a given monthly rain map from the two products. The plot shown covers the period of 1 Jul–31 Dec 1999. Also shown is the regression equation between the two estimates as well as their correlation.

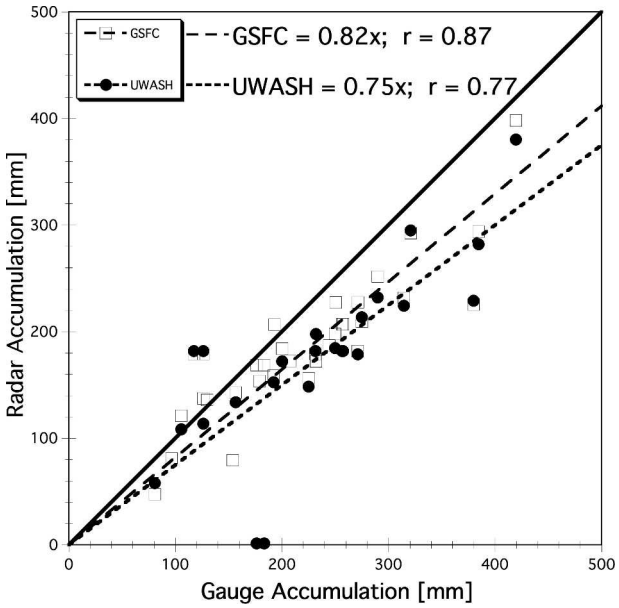

FIG. 16. Scatterplot of TSVO and UWASH monthly rainfall estimates above gauges vs the observed rainfall by those gauges. Also shown are the respective regression equations and correlations.

mates are about 8% higher than UWASH estimates. The difference of the ratios in level II (13%) and level III (8%) are probably due to differences in the accumulation algorithm used by the two groups. The main factor affecting the differing integration techniques is due to the presence of radar data gaps (periods when the radar was not operating).

h. Comparison of radar estimates to gauge observations

Figure 16 is a scatterplot of TSVO and UWASH versus gauge observations. Recalling that UWASH uses a single time-independent disdrometer-based power-law Z_e–R relationship and that TSVO uses a WPMM Z_e–R derived from data in 2002, the following can be stated: 1) both of the comparisons provide independent validation; 2) both are well correlated, with TSVO and UWASH correlations of 0.87 and 0.77, respectively; and 3) the TSVO and UWASH estimates are approximately 18% and 25% low relative to the gauge observations, respectively. No attempt is made here to state which estimates might be closer to the "truth," given the limited quantity and quality of gauge data at KWAJ. It has been determined that the differences between the GSFC estimates and the gauge accumulations can be attributed to a radar calibration of only 1 dB. Houze et al. (2004, manuscript submitted to *J. Appl. Meteor.*) state that they applied a +6 dB correction to the KWAJ reflectivity data prior to conversion to rain rate, while TSVO applied only +5 dB. After application of the additional +1 dB to the TSVO reflectivities, the R/G ratio was increased from 0.87 to 0.97 and the mean absolute difference decreased from 0.21 to 0.18, both significant improvements.

5. Comparisons to TRMM satellite estimates

Finally, we provide a brief review of how well the GV estimates compare to TRMM satellite-retrieved estimates. We note that the TRMM data used in this analysis is from the version 6a algorithms over the period January 2001 through April 2002 and do not represent the "official" version 6 estimates. The TRMM Science Data and Information System (TSDIS) is currently processing the official products, and thus they are not available for comparison at the time of this writing. From information provided by the algorithm developers, we do not believe that there will be significant changes in these comparisons for over ocean; however, there may be some significant differences in the comparisons over land and coast and thus must be addressed in future research.

For brevity, we provide comparisons of our GV estimates over KWAJ and MELB only. For this analysis, estimates from the TRMM gridded 3G-68 product were used to compare to GV rain intensities. The 3G-68 global product provides the average rain rate in 0.5° × 0.5° pixels for the TMI, PR, and COM algorithms. Each 3G-68 pixel that lies over the respective GV sites was

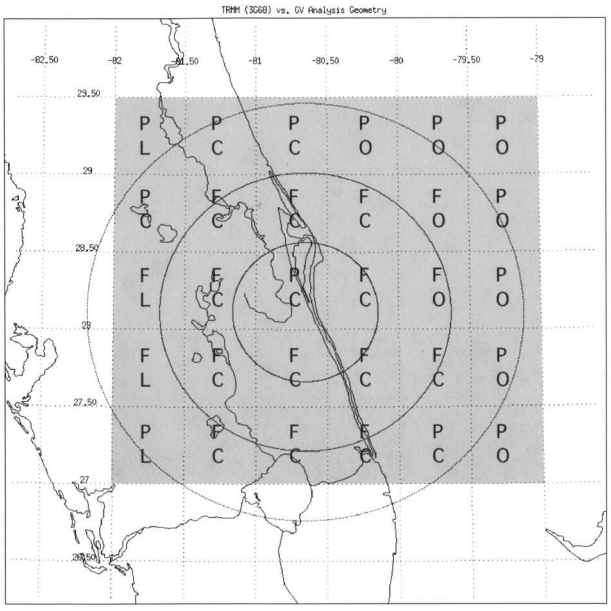

FIG. 17. Mask used for comparing TRMM and GV instantaneous rates. Each pixel is a 0.5° × 0.5° box: "L" represents land, "C" represents coast, "O" represents ocean, "P" represents pixels that contain more than one distinct geographical type (L, C, or O), and "F" represents pixels that contain only one geographical type and are fully within the radar domain (i.e., less than 150 km).

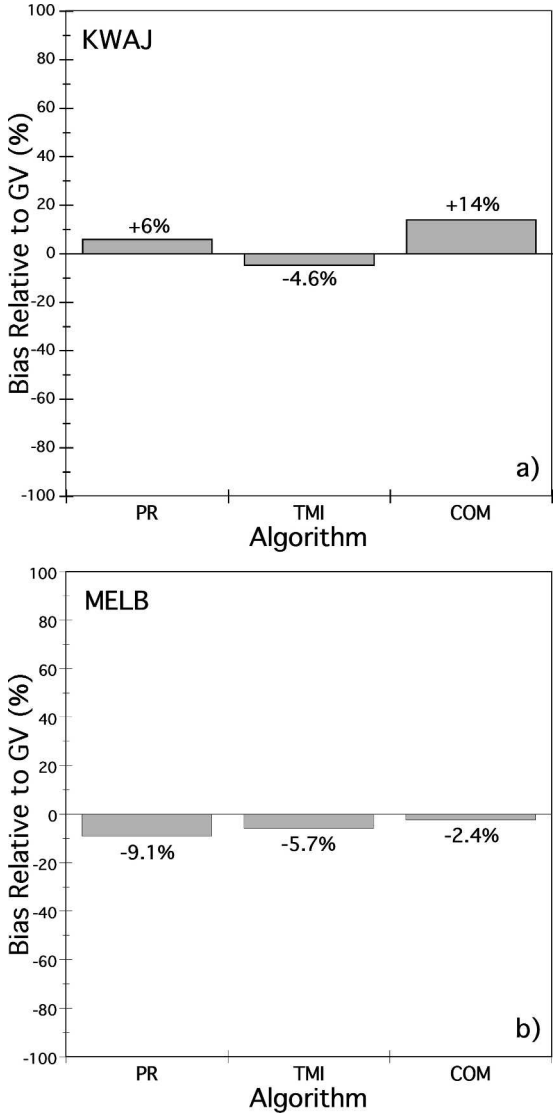

FIG. 18. Bias of TRMM satellite estimates relative to GV for the period Jan 2001–Apr 2002 for (a) KWAJ and (b) MELB. These biases are calculated by comparing the mean rain rate over 0.5° × 0.5° pixels in the GV domain. Only pixels that were considered as "ocean" by the TRMM satellite algorithms are shown. The bias is defined as the difference between the GV and satellite and GV mean for the period, normalized to the GV mean, and is expressed in Eq. (1) in the text.

extracted and then compared to TRMM GV estimates obtained by de-resolving the 2 km × 2 km 2A-53 rain map pixels to the same grid as the 3G-68 product. Thus, the comparison was pixel-matched in both time and space, removing sampling as a source of error in these comparisons.

The data from each site were grouped into subsets to provide comparisons over land, coast, and ocean (Fig. 17). For KWAJ, there are no land or coast pixels, as it is considered solely oceanic. The bias, defined in Eq. (1), provides a bulk estimate of the agreement between GV and the satellite estimates. In Eq. (1), satellite is the TRMM estimate (PR, TMI, or COM), and GV is the ground validation:

$$\text{bias} = \frac{\text{satellite} - \text{GV}}{\text{GV}}. \quad (1)$$

Calculating a "bulk" bias [Eq. (1)], using all 0.5° pixels in which there was at least one PR footprint and a fully contained valid GV region, the TRMM estimates match well with GV estimates over open ocean (Fig. 18). For KWAJ (see Fig. 3a), the PR, TMI, and COM estimates were +6%, −4.6% and +14% of GV estimates, respectively. For MELB (see Fig. 3b), the PR, TMI, and COM estimates were –9.1%, −5.7%, and –2.4% of GV estimates, respectively. Thus a strong convergence is evident not only in the TRMM satellite estimates, but also between TRMM and GV.

Over land and along the coastal areas, there are substantial differences between the various TRMM algorithms; however, it is our understanding that the official version 6 products will mitigate some of these differences. Current research and future efforts will provide considerably more detail on the effectiveness of the GV estimates in validating TRMM, but it suffices to say here that the latest products for GV and the satellite have converged to a point that have nearly achieved the early prognostications of 10% error over a 5° × 5° box on a monthly scale by North et al. (1987).

A detailed discussion on the regional and physical

differences between the various TRMM algorithms is beyond the scope of this paper; however, work is underway now to provide similar validation on a satellite "footprint" scale in order to better understand why the apparent regional differences in the estimates occur (C. Kummerow 2003, personal communication).

6. Summary and conclusions

An overview of the Tropical Rainfall Measuring Mission (TRMM) Ground Validation Program is presented. The validation program, based at NASA Goddard Space Flight Center in Greenbelt, Maryland, is responsible for processing several TRMM science products for validation space-based rain estimates from the TRMM satellite. These products include gauge rain rates, radar rain intensity, precipitation type, and rain accumulations. The rain intensity estimates are derived using the Window Probability Matching Method (WPMM), which matches the probabilities of radar-observed reflectivities Z_e and gauge-measured rain intensity R in such a way that the PDF of the radar-estimated R above the gauge will be identical to the PDF of the gauge rates on a monthly scale. The resulting Z_e–R functions are curved lines in log–log space rather than a straight-line power law. A comparison of the NASA GV program products and those developed by the University of Washington for a subset of data from one of the sites (Kwajalein, Republic of the Marshall Islands) is presented, and it is shown that the two estimates are near 10% of one another on both instantaneous and monthly time scales. It is shown that, for the period July–December 1999, both the NASA and UWASH estimates are lower than the gauge-measured monthly rain totals by 18% and 25%, respectively. Finally, a brief comparison of NASA GV rain intensities to satellite retrievals from the TRMM Microwave Imager (TMI), Precipitation Radar (PR), and Combined (COM) algorithms is presented, and it is shown that the GV and satellite estimates agree quite well over ocean. At Kwajalein, all three satellite estimates are well within 10% of GV estimates, while at Melbourne, Florida, both the TMI and PR are within 10% of GV estimates and the COM algorithm is approximately 14% higher than the GV estimates. Further research on the official version 6 products will be conducted when that data become available some time in 2005.

Acknowledgments. The authors thank Dr. Ramesh Kakar (NASA Headquarters), Dr. Robert Adler (TRMM Project Scientist), and Mr. Richard Lawrence (Chief, TRMM Satellite Validation Office) for their guidance and support of this effort. We also appreciate the support staff of the TSVO, including David Makofski, Bart Kelley, David Augustine, Marcella Shupp, and Karen Mitchell.

REFERENCES

Amitai, E., 2000: Systematic variation of observed radar reflectivity–rainfall rate relations in the Tropics. *J. Appl. Meteor.,* **39,** 2198–2208.

——, D. B. Wolff, M. Robinson, D. S. Silberstein, D. A. Marks, M. S. Kulie, and B. Fisher, 2001: Methodologies for evaluating the accuracy of TRMM ground validation rainfall products. Preprints, *30th Int. Conf. on Radar Meteorology,* Munich, Germany, Amer. Meteor. Soc., 363–365.

——, ——, D. A. Marks, and D. S. Silberstein, 2002: Radar rainfall estimation: Lessons learned from the NASA/TRMM validation program. *Second European Conference on Radar Meteorology (ERAD),* ERAD Publication Series, Vol. 1, Copernicus, 255–260.

——, J. A. Nystuen, L. Liao, R. Meneghini, and E. Morin, 2004: Uniting space, ground and underwater measurements for improved estimates of rain rate. *IEEE Geosci. Remote Sens. Lett.,* **1,** 35–38.

——, L., Liao, X. Llort, and R. Meneghini, 2005: Accuracy verification of spaceborne radar estimates of rain rate. *Atmos. Sci. Lett.,* in press.

Anagnostou, E. N., C. A. Morales, and T. Dinku, 2001: The use of TRMM Precipitation Radar observations in determining ground radar calibration biases. *J. Atmos. Oceanic Technol.,* **18,** 616–628.

Atlas, D., 1987: Early foundations of the measurement of rainfall by radar. *Radar in Meteorology: Battan Memorial and 40th Anniversary Radar Meteorology Conference,* D. Atlas, Ed., Amer. Meteor. Soc., 86–97.

——, D. Rosenfeld, and A. R. Jameson, 1997: Evolution of radar rainfall measurements: Steps and mis-steps. *Weather Radar Technology for Water Resources Management*, B. Braga and O. Massambani, Eds., UNESCO, 1–60.

Austin, P. M., 1987: Relation between measured radar reflectivity and surface rainfall. *Mon. Wea. Rev.,* **115,** 1053–1070.

Ciach, G. J., W. F. Krajewski, E. N. Anagnostou, M. L. Baeck, J. A. Smith, J. R. McCollum, and A. Kruger, 1997: Radar rainfall estimation for ground validation studies of the Tropical Rainfall Measuring Mission. *J. Appl. Meteor.,* **36,** 735–747.

Crum, T. D., R. L. Alberty, and D. W. Burgess, 1993: Recording, archiving, and using WSR-88D data. *Bull. Amer. Meteor. Soc.,* **74,** 645–653.

Doviak, R. J., 1983: A survey of radar rain measurement techniques. *J. Climate Appl. Meteor.,* **22,** 832–849.

Gray, W., and R. W. Jacobson, 1977: Diurnal variation of deep cumulus convection. *Mon. Wea. Rev.,* **105,** 1171–1188.

Habib, E., and W. F. Krajewski, 2002: Uncertainty analysis of the TRMM ground-validation radar-rainfall products: Application to the TEFLUN-B field campaign. *J. Appl. Meteor.,* **41,** 558–572.

——, ——, and A. Kruger, 2001: Sampling errors of tipping-bucket rain gauge measurements. *J. Hydrol. Eng.,* **6,** 159–166.

Hendon, H. H., and K. Woodberry, 1993: The diurnal cycle of tropical convection. *J. Geophys. Res.,* **98,** 16 623–16 637.

Keenan, T. D., and R. E. Carbone, 1992: A preliminary morphology of precipitation systems in tropical northern Australia. *Quart. J. Roy. Meteor. Soc.,* **118,** 283–326.

Keenan, T., K. Glasson, F. Cummings, T. S. Bird, J. Keeler, and J. Lutz, 1998: The BMRC/NCAR C-band polarimetric (C-POL) radar system. *J. Atmos. Oceanic Technol.,* **15,** 871–886.

Kraus, E. B., 1963: The diurnal precipitation over the sea. *J. Atmos. Sci.,* **20,** 551–556.

Kulie, M. S., M. Robinson, D. A. Marks, B. S. Ferrier, D. Rosenfeld, and D. B. Wolff, 1999: Operational processing of ground validation data for the Tropical Rainfall Measuring Mission. Preprints, *29th Int. Conf. on Radar Meteorology*, Montreal, QC, Canada, Amer. Meteor. Soc., 736–739.

Kummerow, C., W. Barnes, T. Kozu, J. Shiue, and J. Simpson,

1998: The Tropical Rainfall Measuring Mission (TRMM) sensor package. *J. Atmos. Oceanic Technol.,* **15,** 809–817.

Marks, D. A., and Coauthors, 2000: Climatological processing and product development for the TRMM Ground Validation program. Physics and chemistry of the Earth, (PCE), Part B. *Hydrol., Oceans Atmos.,* **25,** 871–876.

North, G. R., 1987: Sampling studies for satellite estimate of rain. Preprints, *10th Conf. on Probability and Statistics in Atmospheric Sciences,* Edmonton, AB, Canada, Amer. Meteor. Soc., 129–135.

Rosenfeld, D., D. Atlas, D. B. Wolff, and E. Amitai, 1992: Beamwidth effects on *Z–R* relations and area integrated rainfall. *J. Appl. Meteor.,* **32,** 50–72.

——, D. B. Wolff, and E. Amitai, 1994: The window probability matching method for rainfall measurements with radar. *J. Appl. Meteor.,* **33,** 682–693.

Schumacher, C., and R. A. Houze Jr., 2000: Comparison of radar data from TRMM satellite and Kwajalein oceanic validation site. *J. Appl. Meteor.,* **39,** 2151–2164.

Simpson, J., C. Kummerow, W.-K. Tao, and R. F. Adler, 1996: On the Tropical Rainfall Measuring Mission (TRMM). *Meteor. Atmos. Phys.,* **60,** 19–36.

Steiner, M., R. A. Houze Jr., and S. E. Yuter, 1995: Climatological characterization of three-dimensional storm structure from operational radar and rain gauge data. *J. Appl. Meteor.,* **34,** 1978–2007.

Wilson, J. W., and E. A. Brandes, 1979: Radar measurement of rainfall—A summary. *Bull. Amer. Meteor. Soc.,* **60,** 1048–1058.

Wolff, D. B., B. L. Fisher, O. W. Thiele, and D. Han, 1995: Diurnal cycle of tropical rainfall based on rain gauge data: Implications for satellite rainfall retrievals. Preprints, *27th Conf. on Radar Meteorology,* Vail, CO, Amer. Meteor. Soc., 743–745.

——, J. Gerlach, B. Fisher, A. Tokay, D. A. Marks, D. S. Silberstein, and J. Wang, 2003: On the characteristics of precipitation in the Florida Keys: The Keys Area Precipitation Project. Preprints, *31st Int. Conf. on Radar Meteorology*, Seattle, WA, Amer. Meteor. Soc., 437–440.